

Effect of Zirconium Doping on Oxidation of Single Crystal β -NiAl

Uran S**Department of Physics, Pittsburg State University, Pittsburg, KS 66762, USA*

Abstract

Relatively new optical techniques are utilized to study the oxidation of low-index crystal faces of a zirconium doped single crystal β -NiAl. With these non-destructive techniques residual stress, phase composition and thickness of the scales were determined at various temperatures. The results are compared with the results obtained from an undoped counterpart. Interesting differences in scale stress, thickness and phase composition have been observed. The residual stress evolves rather differently than that on the undoped counterpart. Initial lower stress levels in the doped crystal convert to higher stresses at higher oxidation temperatures. The orientation dependence and a stress anomaly observed with the undoped single crystal β -NiAl are still present on the doped sample. Fluorescence and Raman results indicate a higher concentration of $\theta\text{-Al}_2\text{O}_3$ on all crystallographic phases with Zr doping. The oxide scales are also thinner on the Zr doped specimen.

Keywords: Alumina scales; Residual stress; Single crystal; Fluorescence; Oxidation; NiAl; Reactive element effect

Introduction

In an article we presented a study of the dependence of oxidation on a single crystal β -NiAl [1]. Since the background material (choice of material, technological relevance, and techniques employed for this investigation is identical [1] it will not be reproduced here.

Intermetallic compound NiAl has potential for being used as high temperature structural material in aerospace engineering [2] or as surface coating for superalloys and turbine blades [3,4] however, it suffers from brittleness and poor oxidation properties.

Addition of small amount (~ 0.1 atm.%) of reactive elements (e.g. Zr, Y, Hf) to substrate materials prior to oxidation is known to greatly improve the oxidation properties (e.g., adherence) of these materials, known as reactive element effect [5-7]. The purpose of this investigation is to determine the role of reactive element doping during oxidation of a single crystal. It can be argued that observance of grain boundaries in the underlying metal might change or inhibit the improved scale adherence normally produced by doping with a reactive element.

By comparing the effects of reactive element doping on the oxidation of different crystallographic faces, we expect to improve our understanding of this still very poorly understood phenomenon. In this study, we have measured scale thickness, composition, and residual stress as a function of oxidation temperature for the three principal low-index surfaces, (001), (110) and (111) of zirconium doped specimen. Systematic differences are observed among different surfaces and the results are compared to those of the undoped crystal.

The optical characterization techniques used in this study are relatively new and non-destructive. The scale thickness was determined from reflectivity measurements, scale composition from ruby and Raman spectroscopy and residual stress from ruby fluorescence. The results are given in the following section.

Experimental Details and Results

Sample preparation

The specimen studied was a nominally stoichiometric 0.1 atm.% zirconium doped single crystal ingot of β -NiAl. A homogeneous mixture of Ni-Al (0.1 atm.% Zr) were obtained by arc-melting Ni, Al and Zr into small (~ 5 cm 3) buttons. These buttons were then placed

in a crucible which was inserted into a programmable furnace. The specimen was heated to 1677°C, just above the melting point (1640°C) of NiAl. After melting, the specimen was slowly cooled at a rate of 2°C per hour. We observed two large grains with our samples. The single crystal nature of the resulting β -NiAl (0.1 atm.% Zr) ingot was ascertained using Laue x-ray diffraction techniques. Even though some of the Zr segregated into the single grain boundary, approximately 0.05-0.07 atm.% was still detected in the single crystal by SEM and EDX measurements. Finally, the crystallographic surfaces (001), (111), (110) were oriented and polished with 1- μm diamond suspension. An unoriented surface was also polished for comparison. Prior to oxidation, the specimen was cleaned in acetone and alcohol.

The β -NiAl (0.1 atm.% Zr) ingot was oxidized for one hour at each temperature with 100°C increments from 300°C to 1200°C and with 50°C increments from 1250°C to 1450°C. This rather unusual heat treatment schedule is chosen because it provides information at many different temperatures. Conversely, since the oxide scale is accumulative, it suffers from the disadvantage that there could be effects arising from the lower temperature oxidation. Nonetheless, given the rather rapid increase in oxidation as the temperature is raised, we feel that the approach is warranted for these initial experiments. After each oxidation, the sample was cooled by quenching in air. Stress, scale thickness and composition measurements were all performed ex-situ at ambient temperature.

Fluorescence studies

Residual stresses in thermally-grown-alumina scales can be determined by employing ruby fluorescence spectroscopy. The details of the technique, measurement and stress calculation [1]. In Figure 1 we present ruby spectra recorded on the (001) face of both doped and undoped β -NiAl oxidizing the specimens one hour at 1200°C. An unstressed ruby spectrum is also shown as a reference in the same

*Corresponding author: Serif Uran, Department of Physics, Pittsburg State University, Pittsburg, KS 66762, USA, Tel: (620) 235 4395; E-mail: suran@pittstate.edu

Received January 05, 2018; Accepted February 01, 2018; Published February 10, 2018

Citation: Uran S (2018) Effect of Zirconium Doping on Oxidation of Single Crystal β -NiAl. J Material Sci Eng 7: 424. doi: [10.4172/2169-0022.1000424](https://doi.org/10.4172/2169-0022.1000424)

Copyright: © 2018 Uran S. This is an open-access article distributed under the terms of the Creative Commons Attribution License, which permits unrestricted use, distribution, and reproduction in any medium, provided the original author and source are credited.

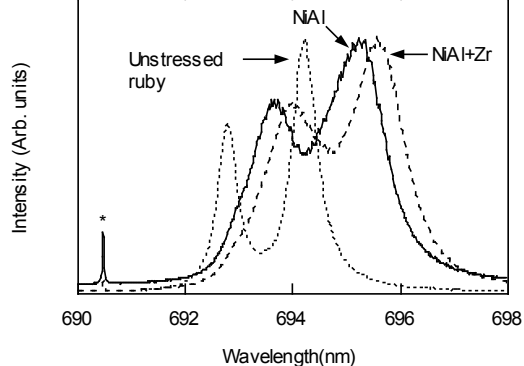


Figure 1: Ruby spectra on the (001) surface of both doped and undoped β -NiAl after oxidizing the specimens one hour at 1200°C.

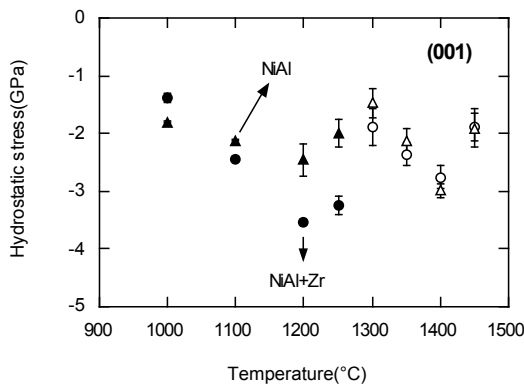


Figure 2: Hydrostatic stress versus temperature for the (001) surface.

figure. The (001) surfaces show a difference in their scale-stress state; doped specimen exhibits higher stress values at this temperature. The star in the figure refers to a Kr line used for calibration purposes. The overall hydrostatic scale-stress versus temperature results obtained on the (001) face of both doped and undoped β -NiAl are shown in Figure 2. The plot shows that the residual stress has a different trend for the two crystallographically identical faces. Open circles in the plot indicate that the scale was visibly flaking off; a clear sign that spallation, stress relaxation, and/or regrowth must be occurring. Under these conditions the spot to spot variations are considerably larger as indicated by the error bars. Figure 3 shows the hydrostatic residual stress versus temperature results for the (110) surface of the two specimen. The residual stresses evolve quite differently on two faces; the Zr doped specimen exhibit lower scale-stress below 1200°C and higher scale-stress above this temperature. The stress anomaly observed at around 1250°C with the undoped β -NiAl is still present with the Zr doped counterpart, but somewhat postponed to higher temperature. Figure 4 presents equivalent results for a (111)-oriented surface of the two specimens. Although the results are similar to those obtained with the (110) face, the stress anomaly is rather different. The open triangle indicates a stress relief via cracking and/or flaking off. We have also investigated the behavior of an unoriented surface on the two specimens. In Figure 5 hydrostatic scale stress is plotted as a function of temperature for these surfaces. The two surfaces exhibit quite different scale-stress behavior; being (001)-like (i.e., cracking and/or flaking off) for the undoped specimen and sustaining high amounts of stress on the

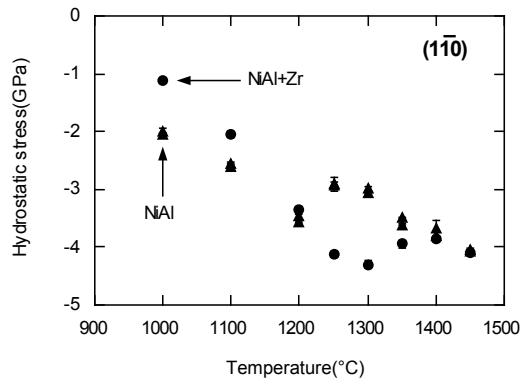


Figure 3: Hydrostatic stress versus temperature for the (110) surface.

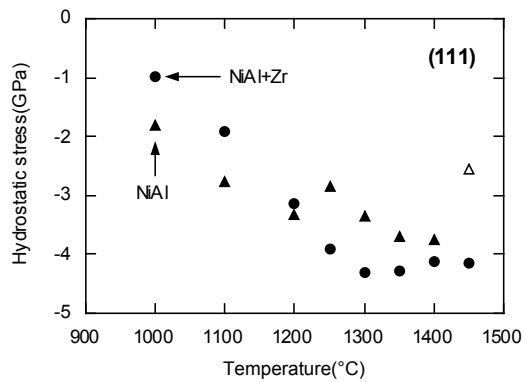


Figure 4: Hydrostatic stress versus temperature for the (111) surface.

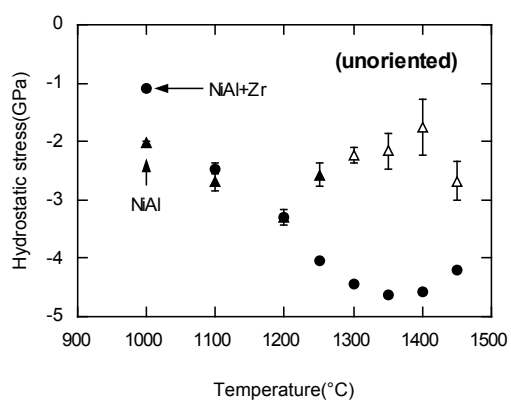


Figure 5: Hydrostatic stress versus temperature for an unknown high index surface.

doped specimen. The above mentioned anomaly is also present on the unoriented surface of the Zr doped specimen above 1350°C.

In order to better compare the orientation dependence, the hydrostatic stress values obtained on the undoped specimen have been normalized to that on the Zr doped specimen for each crystallographic face and temperature. The results are plotted in Figure 6. There appears to be a dip at ~1250°C for the (111), (001), and (110) faces (Figure 6a-c). The ratio yields similar results on the (111) and (110) faces, but the (001) face of the Zr doped specimen exhibits higher residual stresses

compared to that of the undoped specimen at lower temperatures. Also one needs to keep in mind that the (001) surface of both specimens exhibit scale flake off above 1250°C. However, the (111) and (110) faces do not show this behavior. Not surprisingly, the unoriented faces which are not really comparable appear to have a different trend in the ratio above 1250°C (Figure 6d) partly because there is scale cracking and/or spallation on the undoped specimen.

Since the thermal expansion of cubic NiAl is isotropic the differences observed above cannot be attributed to differences in thermal expansion. One possible origin for the differences is a change in the growth stresses induced by epitaxial constraints on each surface.

Raman results

With currently available CCD detectors, Raman scattering becomes a convenient and practical optical technique for the characterization of oxide films on metals and alloys [8]. Since the technique is insensitive to the underlying metal or alloy substrate, the resulting information pertains only to the oxide scales and provides direct identification of compounds within the scale. In particular, the technique can be used to monitor the evolution of transient oxide phases prior to the formation of the final protective scale. Raman scattering measures optical phonons, which are the normal modes of atomic vibration in a material. Since each material has its own "fingerprint" spectrum for these vibrations, they can be used to identify and track the evolution of various constituents in the oxide scale. In Figure 7, the evolution of Raman spectra measured on the (001) surface, after oxidation at temperatures in the 800°C to 1450°C range, are plotted. Our oxidation steps of the β -NiAl+Zr are the same as those on the undoped counterparts. For treatments between 300°C to 700°C there are no distinct features in the Raman spectra. However, the increasing background observed on the undoped specimen in the 800-1000°C range [1] is absent on the doped specimen.

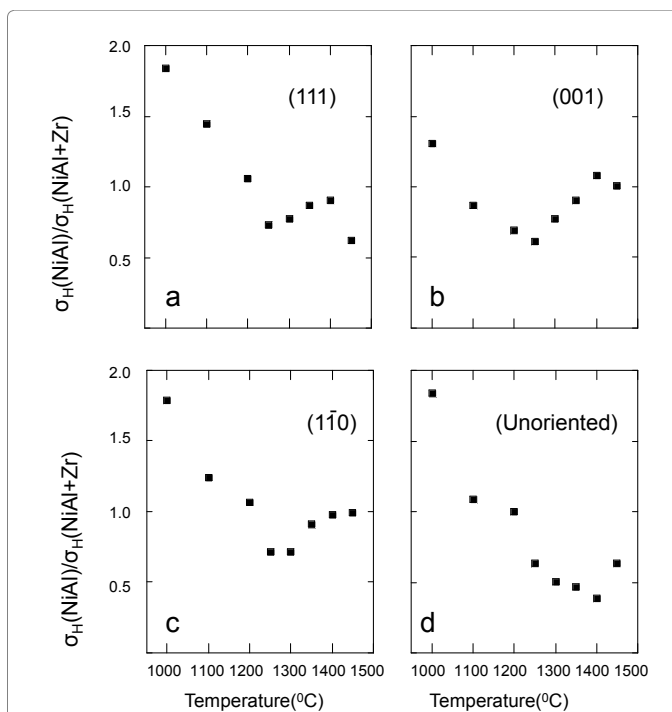


Figure 6: Hydrostatic stress ratio of scales on doped and undoped β -NiAl single crystals for various crystal surfaces.

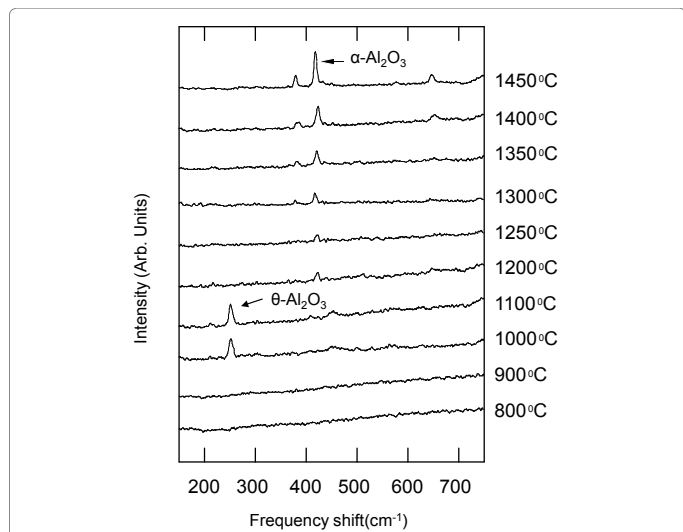


Figure 7: The evolution of Raman spectra measured on the (001) surface after heat-treatments 800°C to 1450°C range.

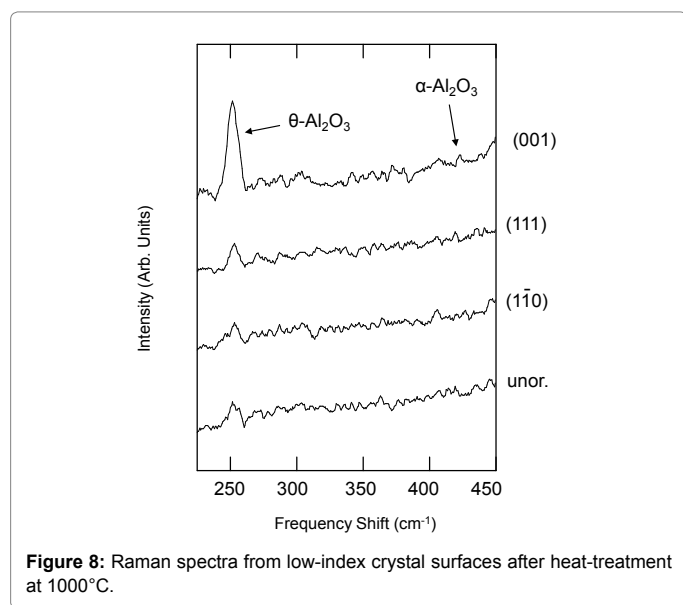


Figure 8: Raman spectra from low-index crystal surfaces after heat-treatment at 1000°C.

The first clearly identifiable Raman peak is observed at 1000°C. This peak, at around 252 cm^{-1} , has been ascribed to the $\theta\text{-Al}_2\text{O}_3$ phase [9]. This phase persists at 1100°C and the corresponding signal is more intense compared to that of the undoped specimen. An $\alpha\text{-Al}_2\text{O}_3$ peak at $\sim 423 \text{ cm}^{-1}$ starts to be detectable at 1200°C and continues to grow gradually after oxidation at 50°C increments. For all temperatures studied, the $\alpha\text{-Al}_2\text{O}_3$ signal is more intense on the undoped sample. Raman spectra from different surfaces, after oxidation at 1000°C, are plotted in Figure 8 where it can be seen that the (001) surface contains considerably more of the θ phase than the other surfaces, a result which was also observed on the undoped counterpart. No $\alpha\text{-Al}_2\text{O}_3$ is observed in the 1000°C spectra with the Raman measurements.

Figure 9 shows Raman spectra from each orientation after oxidation at 1100°C. The asterisk represents a plasma line from the laser and should be ignored. It is clear from the figure that the (001) face still contains considerable amount of $\theta\text{-Al}_2\text{O}_3$ whereas the (111), (110) and unoriented faces do not show any detectable amount of this

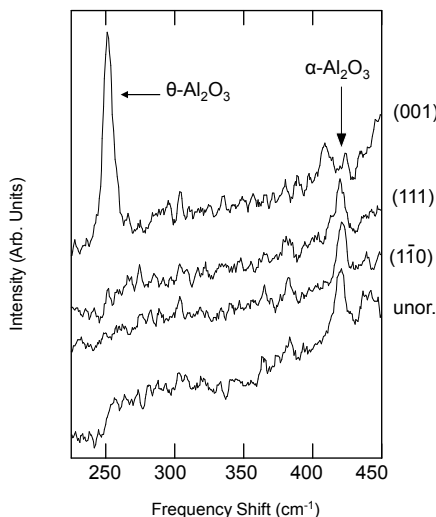


Figure 9: Raman spectra from low-index crystal surfaces after heat-treatment at 1100°C.

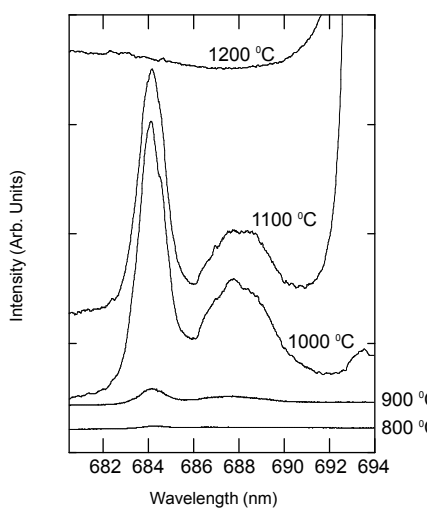


Figure 10: Fluorescence spectra recorded on the (001) surface at five temperatures 800-1200°C.

particular transient phase. The $\alpha\text{-Al}_2\text{O}_3$ signal is clearly observable and stronger on the (111), (110) and unoriented faces than on the (001) face showing that the composition of the scale evolves quite differently on the various surfaces. This result was also observed with the undoped counterparts, providing a strong support for the reproducibility of the obtained results. Here, we emphasize that the same remarkable trends in $\theta\text{-Al}_2\text{O}_3$ and $\alpha\text{-Al}_2\text{O}_3$ compositions on these crystallographic faces were also observed with the undoped specimen.

Fluorescence from transient Al_2O_3 phases

The Raman results presented in Part C provide information on the oxide phase composition of the scale. Fluorescence also yields information on the phase composition. The sloping background observed at low temperatures with the undoped β -NiAl [1] is absent with the Zr doped counterparts (Figure 7). We remind reader that this sloping background is most likely a fluorescence signature of a transient oxide that we have not identified. Nevertheless, another fluorescence

signal reported [10] close to the ruby doublet and attributed to $\theta\text{-Al}_2\text{O}_3$ is present above 900°C. Figure 10 presents the corresponding spectra recorded on the (001) surface of the Zr doped specimen at temperatures spanning 800°C-1200°C. The spectra indicate how the $\theta\text{-Al}_2\text{O}_3$ signal is small at 900°C, a maximum around 1000°C and zero at 1200°C. This result has also been achieved with the undoped β -NiAl and consistent with the known transformation of $\gamma\text{-Al}_2\text{O}_3$ to $\theta\text{-Al}_2\text{O}_3$ to $\alpha\text{-Al}_2\text{O}_3$ as a function of temperature [11]. An interesting point to make here is that the (001) surface on Zr doped β -NiAl contains approximately four times more of the θ phase than that on the undoped counterparts, which is consistent with the known retardation effects of reactive element doping [12]. Figure 11 presents spectra in the θ fluorescence region for the sample heated to various temperatures. At 800°C we observe that the θ phase signal is the strongest on the (001) surface and weakest on the (111) surface. After the 900°C and 1000°C treatments the strongest signal is observed on the (001) face and the weakest on (111). After treatment at 1100°C the (001) face is the only surface on which $\theta\text{-Al}_2\text{O}_3$ is still present. These results were consistently observed

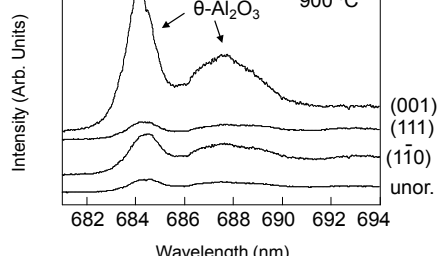
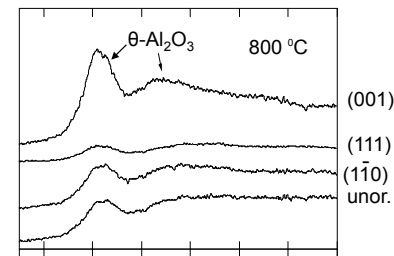
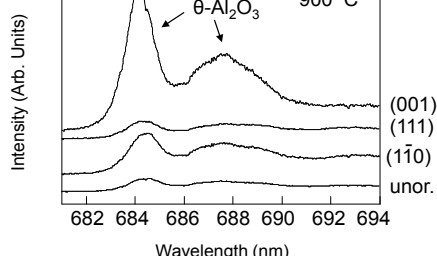
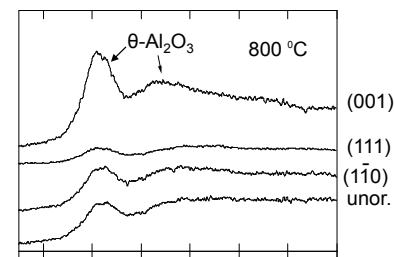


Figure 11: (a and b) Fluorescence spectra from low-index crystal surfaces at four temperatures 800-1100°C.

on the undoped β -NiAl as well, but the overall θ signal is approximately four times stronger on the Zr doped counterpart. These results confirm the conclusion reached based on the Raman data.

Thickness results

The reflectivity of above crystallographic surfaces is measured and normalized to reflection from a mirror by a CARY spectrometer that covers from the near IR to the near UV (3300 to 45000 cm^{-1}) region. Typical reflectivity curves are shown in the inset of Figure 12. The extracted scale thickness is plotted as a function of temperature for the various crystal surfaces in Figure 12. The scale thicknesses for different crystallographic faces and temperatures are summarized in Table 1. For comparison purposes, we also present the equivalent thickness results obtained on the undoped specimen in Table 2. We observe that the overall scale thicknesses on the Zr doped specimen are thinner than those on the undoped specimen [1]. Especially at temperatures above 1200°C , large thickness differences have been observed between the two samples; the scales on the undoped specimen are as much as three times thicker than that on the Zr doped one. As we observed on the undoped sample, the thickness increases slowly up to 1300°C and rapidly above this temperature. The roughness of the scales prevents any thickness measurements above 1400°C .

To better highlight the difference in behavior between the various surfaces at each temperature, we present scale thickness ratio (i.e., NiAl/(NiAl+Zr)) of the two specimen in Figure 13. The scale thicknesses on all crystallographic surfaces of undoped specimen are thicker than that on the Zr doped specimen at all temperatures. The thickness ratios for different faces are roughly constant below 1250°C . Above this temperature an increase in the ratio is observed for all faces except the (001) face where no data is available due to extensive scale flake off. As much as three times thicker scales are measured on the (111) face of

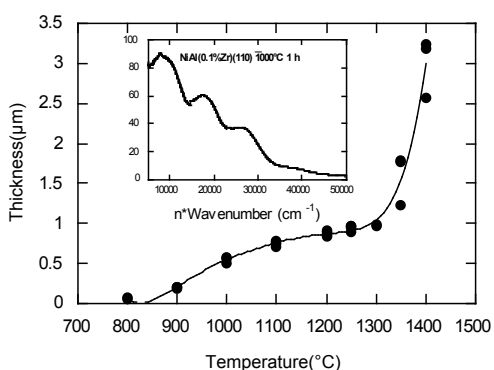


Figure 12: Scale thickness versus temperature for the various crystal surfaces. The inset shows a typical reflectivity curves.

Temperature (°C)	(001)	(111)	(110)	(Unoriented)
800°C	0.063	0.065	0.066	0.067
900°C	0.18	0.21	0.21	0.21
1000°C	0.51	0.57	0.56	0.57
1100°C	0.74	0.77	0.71	0.79
1200°C	0.89	0.85	0.83	0.91
1250°C	0.97	0.98	0.90	0.95
1300°C		0.99	0.99	0.97
1350°C		1.23	1.79	1.77
1400°C		3.19	2.57	3.24

Table 1: Zr doped β -NiAl scale thicknesses for different crystallographic faces in the temperature range 800°C to 1400°C .

Temperature (°C)	(001)	(111)	(110)	(11̄0)	(unoriented)
800°C	0.066	0.087	0.070	0.068	0.067
900°C	0.21	0.29	0.32	0.30	0.28
1000°C	0.64	0.71	0.73	0.72	0.82
1100°C	0.98	0.90	0.99	0.96	1.06
1200°C	1.15	1.17	1.14	1.12	1.24
1250°C	1.50	1.63	1.55	1.53	1.58
1300°C		2.74	2.51	2.52	2.58
1350°C		4.30	3.90	3.96	
1400°C			5.64	5.66	

Table 2: Undoped β -NiAl scale thicknesses on different crystallographic faces in the temperature range 800°C to 1400°C .

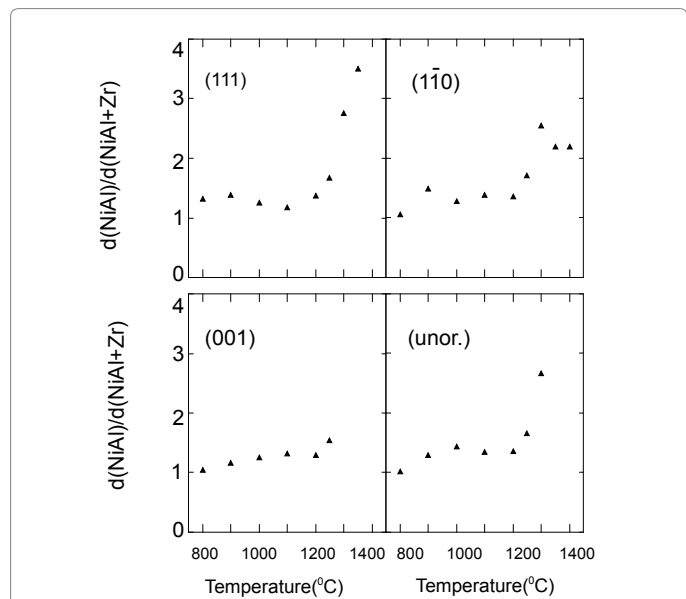


Figure 13: Thickness ratio of scales on doped and undoped β -NiAl single crystal for various crystallographic surfaces.

the undoped specimen compared to that on the Zr doped counterpart at 1350°C .

Raman and fluorescence intensities

The intensity of the ruby signal was studied as a function of temperature for both Zr-free and -doped specimens. The results for the (110) surface are presented in Figure 14. Between 1000 - 1200°C , the ruby intensities are stronger on the Zr-doped specimen. However, above 1250°C the intensities are weaker than those on the undoped specimen and in some cases exhibit more than an order of magnitude difference in intensity values. This observation is consistent with the previous studies of our group on reactive element effect [13]. However, the large intensity difference observed between 1000°C and 1400°C do not scale well with the observed thickness change for the two sample. We speculate that most of the change in the ruby intensity results from an increase in the fraction of α - Al_2O_3 in the scale. This can happen by conversion of transient phases to α - Al_2O_3 and/or by direct growth. From the ruby intensity difference between the NiAl alloy that contains Zr versus the respective Zr-free alloy, we conclude that the reactive element must play a role in slowing the conversion of metastable phases to α - Al_2O_3 and/or growth of α - Al_2O_3 . We have also investigated the Raman intensities of the scale on the (110) surface of the Zr-free specimen. The results are presented in Figure 15. The Raman intensity

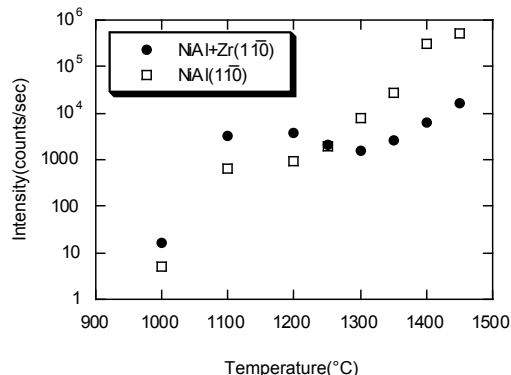


Figure 14: Ruby Intensity versus temperature data for the (110) surface of the Zr-free and doped NiAl.

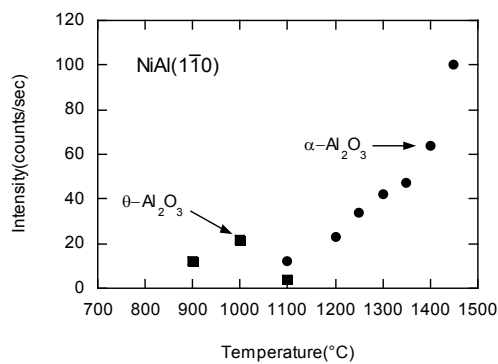


Figure 15: Raman intensity versus temperature data for the (110) surface of the Zr-free NiAl.

change correlates well with the thickness change, providing confidence in our measurements.

Discussion and Comparison with Previous Studies

Reactive element doping of a single crystal β -NiAl has yielded interesting changes on scale stress, thickness and phase composition. Although the oxidation of Zr-doped NiAl was previously compared to its undoped counterparts, experiments were performed on polycrystalline samples with different thermal histories [13-15]. In these experiments, weight change of specimens and scale composition were monitored. Another study investigated only Zr-doped NiAl, measuring composition and weight changes in limited temperature ranges [16]. Most of these studies also utilized very different thermal histories, thereby precluding any comparison. Here we present a study which not only eliminates all these difficulties, but also provides residual stress information in addition to providing scale thickness and composition. In this section we compare, where possible, our results with the above investigations as well as comparing them with the undoped counterpart. We note again that our study was performed on a specimen in which oxide growth at different temperatures was cumulative; this could lead to differences in the oxide growth mechanism compared to that during single temperature oxidation of isothermally cycled samples.

The scale-stress results on both Zr-doped and undoped single crystal β -NiAl provide a valuable contribution to the oxidation studies of these alloys. The results indicate that residual scale stress is different

on two crystallographically identical faces of doped and undoped specimens. An initial higher residual scale-stress values of undoped specimen converts to being lower compared to Zr doped counterparts at higher temperatures. The stress anomaly (i.e., the non-monotonic evolution of stress versus temperature) observed with the undoped specimen is still present with the Zr doped specimen, but somewhat shifted to a higher temperature. Our results show rather interesting trends for different orientations. In both studies, we observe that the (001) surfaces flake off and stress relieve much earlier than the other surfaces, which suggests that the orientation plays an important role during oxidation regardless of the doping. The (111) surface retains its scale integrity even after 1450°C oxidation in the Zr doped specimen, but spalls and stress relieves after 1400°C oxidation in the undoped specimen. The (110) surface, however, retains scale integrity after 1450°C oxidation on both specimens.

The phase composition of scales forming on both Zr-free and doped specimens has been determined from both Raman and fluorescence studies. The overall trend observed in orientation dependence of transient oxidation of Zr-doped β -NiAl single crystal is also reproduced with the undoped counterparts, but the θ - Al_2O_3 content in the scales is approximately four times larger. This could be due to the known retardation effects of reactive element doping. The θ - Al_2O_3 phase is detected in all scales grown between 800 and 1100°C, but the ratio of θ - Al_2O_3 to α - Al_2O_3 depends on both temperature and crystallographic orientation. Above 1100°C, however, only α - Al_2O_3 is detected.

To our knowledge, the effect of doping and temperature dependence of transient oxidation of single crystal β -NiAl has not been studied. There is only one other investigation that concentrated on two different temperature oxidations, namely 800°C and 1100°C, of the transient oxidation of Zr doped β -NiAl single crystal alloys [16]. Mostly, the studies have concentrated upon polycrystalline [7-10]. Zr doped β -NiAl alloy with different compositions. Doychak, et al. [16] characterized the transient oxidation of (0.1 wt.%) Zr doped β -NiAl single crystals, oxidized in air at 800°C and 1100°C, using TEM. They report that the scale contains mainly metastable Al_2O_3 phases and that θ - Al_2O_3 is the major constituent for 10 hours of oxidation at 800°C and 0.1 hours at 1100°C; this result also strongly supports our Raman and fluorescence findings.

Since the crystallographic orientation dependence of transient oxide phases studied as a function of temperature [1]. Our thickness results indicate that the scales on the Zr doped single crystal β -NiAl are thinner than those on the undoped counterparts for all temperatures studied. The thickness difference observed can be attributed to the reactive element effect. It is possible that the Zr addition changes the diffusion properties of the metal-oxide interface and/or the scale by introducing small amounts of ZrO_2 .

There is a rapid scale thickness increase which takes place above \approx 1300°C with the Zr doped specimen and above \approx 1200°C with the undoped counterpart. Even though this rapid thickness increase might be due to the θ - to α - Al_2O_3 phase transformation, this phase transformation as judged by our Raman and fluorescence results appears to be complete at these temperatures.

In the literature, there are only limited number of studies of oxidation kinetics of Zr doped NiAl [7-10]. Since these studies have mostly relied on weight change determinations comparisons with our thickness results will be qualitative rather than quantitative. Barrett et al. [12] using microscopy, observed thicker scales on polycrystalline Zr doped NiAl compared to the undoped counterparts. Although

this contradicts our findings, care must be taken in interpreting this difference since our samples are single crystals and the thermal histories are different. The only study of weight change measurements on Zr doped single crystal β -NiAl was done by Doychak et al. [17] Doychak has observed that the scale on the (001) surface is thinner than that on the (011) surface after 800°C and 1100°C treatments, which is consistent with our findings.

Based on our current results, we are unable to explain the large ruby intensity difference which does not scale well with the thickness difference. The Raman intensity changes, however, correlate well with the thickness change [17].

Summary and Conclusions

We have studied the effect of Zr doping on the oxidation of low-index crystal surfaces of single crystal β -NiAl using relatively new and non-destructive optical techniques. These techniques have proved to be very useful in determining scale stress, composition, and thickness as a function of temperature and in detecting differences in the oxidation behaviors of different crystallographic surfaces.

We can summarize the observations from this study:

(1) Reactive element doping has a considerable effect on the residual scale-stress. The stress anomaly observed with the Zr-free specimen is still present with the doped counterparts, but shifted to higher temperatures. On both specimens, we observe that the (001) surfaces flake off and stress relieve much earlier than the other surfaces, which suggests that the orientation plays an important role on oxidation regardless of the presence of a reactive element. The scale integrity of the (111) surfaces improved greatly by addition of a reactive element,

(2) The phase composition studies of the scales indicate that the reactive element doping has a strong influence on the $\theta\text{-Al}_2\text{O}_3$ concentration. Similar to the observation with the undoped β -NiAl, the (001) surface is the one on which the $\theta\text{-Al}_2\text{O}_3$ is detected at the lowest temperature, has the highest concentration and lasts to the highest temperatures,

(3) Much thinner scales are formed on the Zr doped NiAl compared to those on the undoped counterparts,

(4) Reactive element doping plays a role in slowing conversion of the metastable phases to $\alpha\text{-Al}_2\text{O}_3$ and/or in slowing the growth of $\alpha\text{-Al}_2\text{O}_3$.

From the observation of thinner scales on the Zr doped NiAl, it is clear that the reactive element slows the scale formation. It is likely that there is small amount of ZrO_2 in the scale which changes the diffusion properties.

In spite of the fact that orientation-dependent effects are clearly observed in the oxidation of both Zr doped and undoped single crystal

β -NiAl, the origin of these effects is still not well understood. It is clear nevertheless that the characterization techniques used here provide information previously not easily accessible. We feel that similar studies on other materials, and a variety of thermal conditions will produce valuable contributions to the field of high temperature oxidation.

References

- Uran S, Grimsditch M, Veal BW, Paulikas AP (2001) Optical Investigation of the Effects of Substrate Orientation on Oxidation of Single Crystal β -NiAl. Oxidation of Metals 56: 551-569.
- Bochenek K, Basista M (2015) Advances in processing of NiAl intermetallic alloys and composites for high temperature aerospace applications. Progress in Aerospace Sciences 79: 136-146.
- Wei L, Peng H, Jia F, Zheng L, Guo H (2015) Cyclic oxidation behavior of Hf/Zr co-doped EB-PVD β -NiAl coatings at 1200° C. Surface and Coatings Technology 276: 721-725.
- Tawancy HM (2018) Influence of Superalloy Substrate Composition on the Oxidation Resistance of β -NiAl Diffusion Coating. Metallography, Microstructure, and Analysis 7: 65-76.
- Whittle DP, Stringer J (1980) Improvements in high temperature oxidation resistance by additions of reactive elements or oxide dispersions. Phil. Trans. Roy. Soc. Lond. A 295: 309-329.
- Guo H, Wang D, Peng H, Gong S, Xu H (2014) Effect of Sm, Gd, Yb, Sc and Nd as reactive elements on oxidation behaviour of β -NiAl at 1200° C. Corrosion Science 78: 369-377.
- Tawancy HM (2016) On the Role of Yttrium in Alumina Formers: Comparative Oxidation Behavior of (Ni-Cr-Al)-and (Ni-Cr-Al-Y)-Based Alloys. Oxidation of Metals 86: 371-383.
- Renusch D, Veal B, Natesan K, Grimsditch M (1996) Transient oxidation in Fe-Cr-Ni alloys: A Raman-scattering study. Oxid. met. 46: 365-381.
- Renusch D, Hodges J, Grimsditch M, Jorgensen JD (2001) Pressure dependence of Cr^{3+} fluorescence in θ -alumina. Oxidation of metals 56: 299-311.
- Lipkin DM, Shaffer H, Adar F, Clarke DR (1997) Lateral growth kinetics of α -alumina accompanying the formation of a protective scale on (111) NiAl during oxidation at 1100° C. Applied Physics Letters 70: 2550-2552.
- Mariotto G, Cazzanelli E, Carturan G, Di Maggio R, Scardi P (1990) Raman and X-ray diffraction study of boehmite gels and their transformation to α -or β -alumina. Journal of Solid State Chemistry 86: 263-274.
- Barrett CA (1988) Oxid. Met. 30: 361-391.
- Renusch D, Grimsditch M, Koshelev I, Veal BW, Hou PY (1997) Strain determination in thermally-grown alumina scales using fluorescence spectroscopy. Oxid. Met. 48: 471-495.
- Nesbitt JA, Vinarcik EJ, Barrett CA, Doychak J (1992) Diffusional transport and predicting oxidative failure during cyclic oxidation of β -NiAl alloys. In High Temperature Aluminides and Intermetallics pp: 561-566.
- Barrett CA (1988) Oxid. Met. 30: 361-369.
- Natesan K, Park JH (1989) Corrosion & Particle Erosion at High Temperatures.
- Doychak J, Smialek JL, Mitchell TE (1989) Transient oxidation of single-crystal β -NiAl. Metall. Trans. A 20: 499-518.
- Hindam HM, Smeltzer WW (1980) Growth and Microstructure of $\alpha\text{-Al}_2\text{O}_3$ on β -NiAl. Journal of the Electrochemical Society 127: 1630-1635.